SLAC-PUB-5079
LBL-27683
June 1989
(M)

Z^0 PHYSICS FROM THE MARK II AT THE SLC*

Gerald S. Abrams

Lawrence Berkeley Laboratory
University of California
Berkeley, California 94720

For the MARK II Collaboration

Stanford Linear Accelerator Center
Stanford University, Stanford, CA 94309

ABSTRACT

The MARK II detector has started to take data at the new SLAC Linear Collider. The novel aspects of the accelerator and of the MARK II are briefly described. Displays of event pictures from some of the early-on data are presented to illustrate the quality of the data. A first presentation of the results of an energy scan near the Z^0 mass that is currently in progress shows the expected resonant enhancement near 91 GeV.

Presented at the IX International Conference on Physics in Collision
Jerusalem, Israel, June 19-21, 1989

* This work was supported in part by the Director, Office of Energy Research, Office of High Energy and Nuclear Physics, Division of High Energy Physics of the U.S. Department of Energy under Contract Numbers DE-AC03-76SF00098 and DE-AC0376SF00515.

I. INTRODUCTION

In this talk I will present very recent results from the upgraded MARK II detector at the newest addition to the family of colliders, the SLAC Linear Collider (SLC). Some salient features of the SLC are reviewed in Section II, while Section III is devoted to a description of the MARK II relevant to the data I will present here. Needless to say, the commissioning of the first of a new breed of colliders and the running of a collider detector require a superb team of physicists, operators, technicians and programmers, all working in concert. I wish here to express my appreciation to them.[1]

The hadronic and leptonic events so far acquired by the MARK II are described in Section IV, with discussions on cuts, backgrounds, and efficiencies. Examples are presented in Section V to illustrate the quality of the data. Finally, in Section VI, results are presented for the energy dependence of the cross section obtained near the peak of Z^0.

II. THE STANFORD LINEAR COLLIDER

The SLC was approved to provide e^+e^- collisions near 90 GeV center of mass energy. As this is a new type of collider, I will review some of the novel features of the SLC. Figure 1 shows a schematic layout of the Collider. The electron beam originates at the gun, traverses the 3 kilometer SLAC Linac as it is accelerated to $\approx$ 47 GeV, and then passes through the north collider arc to arrive at the final focus at which point the beam is focussed to a waist $\approx 4\ \mu$ wide. The positron beam originates near the 2/3 point down the Linac where a second e^- beam is kicked by a pulsed magnet onto an e^+ production target. This e^+ beam is transported back to the entrance of the Linac, and is then accelerated and transported through the south collider arc to the final focus. Damping rings are positioned upstream of the Linac to reduce the emittance of the beams prior to acceleration.

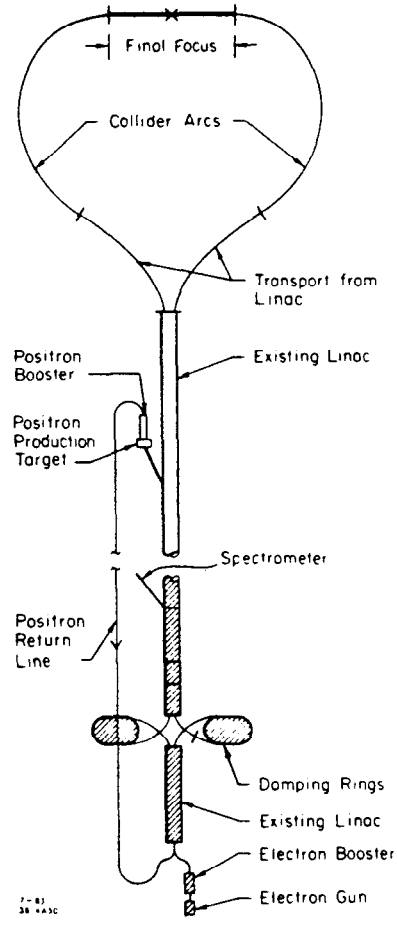

Fig. 1. Schematic layout of the SLC.

In this design beams are made to collide and are then kicked out to deposit the spent beams in dumps. Hence, there is no clean-up of beam tails analogous to the multiple orbits in a storage ring. The primary method

to reduce backgrounds due to tails is to collimate the beams. The collimators and muon "spoilers" (toroids to deflect $\mu^{\pm}$) near the Interaction Point (IP) are shown in fig. 2. This scheme has proved to generate too much debris near the MARK II. Hence, further collimation (see fig. 3) has been introduced upstream to clean up the beams prior to the severe bends into the arcs. Typically $\sim 1/3$ of the beam particles are scraped off at the end of the Linac to achieve suitably small background at the IP.

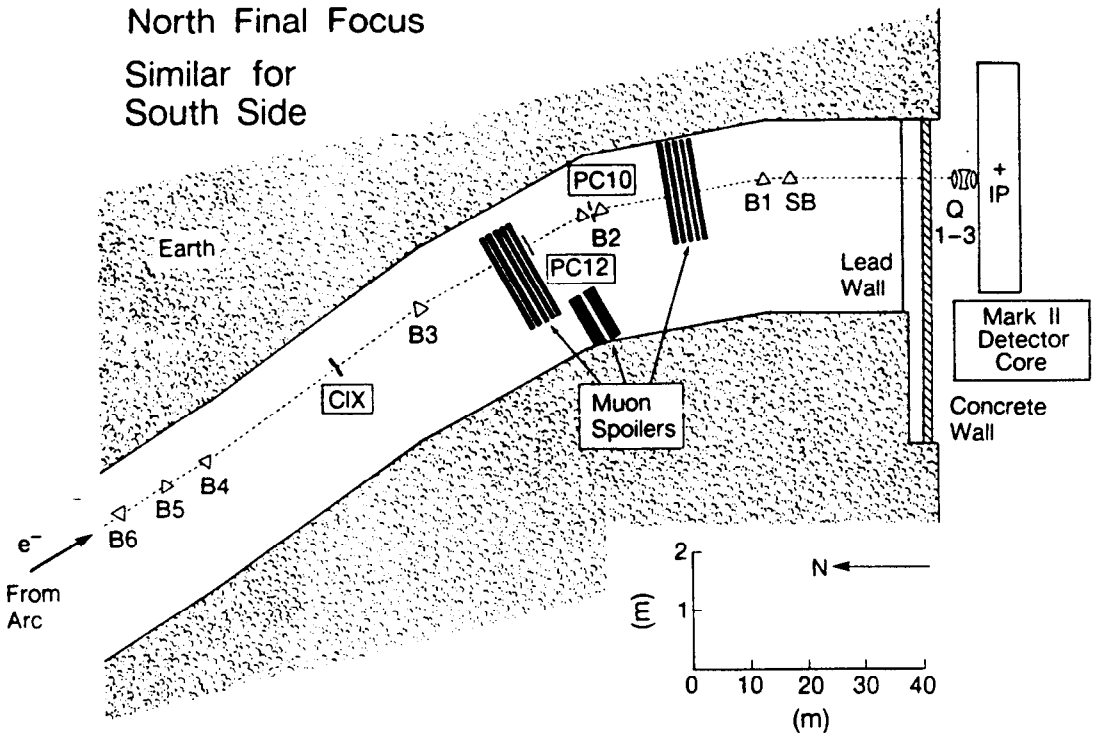

Fig. 2. Collimators and toroids upstream of the IP to reduce background.

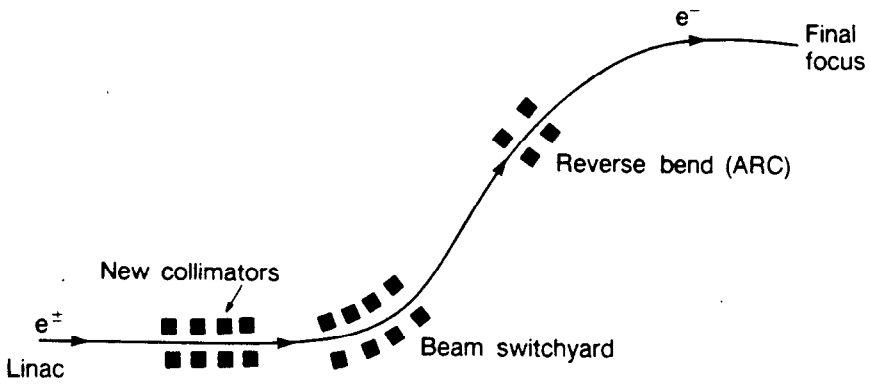

Fig. 3. Additional collimators introduced further upstream in the arcs and the end of the Linac to reduce background.

The principal tool to bring the small ($\sim$ 4 μm) beams into collision at the IP is the beam-beam deflection which uses the macroscopic field of one bunch to deflect the bunch of the on-coming beam. Figure 4 shows the deflection in the horizontal (X) and vertical (Y) directions as the e^+ beam is swept in X position across the e^- beam; for this case the Y displacement had been determined to be $\sim$ 10 μm. The X deflection (fig. 4a) thus shows a deflection which changes sign as the center of one beam is swept through the center of the other, with the magnitude of the deflection being a maximum when the bunch separation is on the order of the bunch sizes. The Y deflection (fig. 4b) shows only the increase in magnitude of deflection as the bunch centers get closer.

A similar deflection sweep for the case where the Y displacement is 0 is shown in fig. 5. The zero crossing point is determined as mid-way between the points of (opposite) maximal deflection, yielding the offset of the target beam. The amplitude of the maximal deflection is a measure of the number of particles in the target bunch; the distance between the maximal deflection points is a measure of the rms size of the two beams; and the slope through the zero crossing is a measure of the luminosity, L.

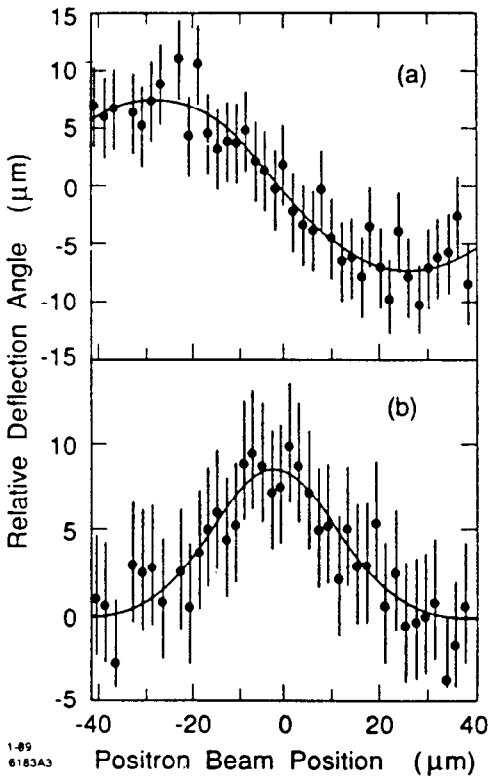

Fig. 4. Measured deflection of the e^+ beam as it is swept in X across the e^- beam (which is displaced 10 μm in Y with respect to the e^+ bunch). a) X deflection. b) Y deflection.

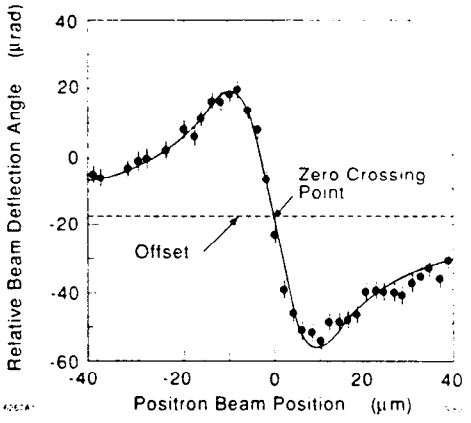

Fig. 5. As in fig. 4a, but here the Y displacement is 0.

The deflection measurements are repeated routinely during data taking to maintain the beams in optimal collision and to provide a detector-independent measurement of the SLC luminosity.

The luminosity of the SLC is determined from the repetition frequency, f, the number of particles $N_{+/-}$ in the e^+/e^- bunches, and the rms beam sizes σ_x and σ_y as

$$L = \frac{f N_+ N_-}{4\pi\sigma_x\sigma_y}.$$

Routine operation during the data collection period of this report had typical parameters of

$$f = 60 \text{ Hz}$$

$$N_+ = N_- = 1 \times 10^{10} \text{ particles/bunch}$$

$$\text{and} \quad \sigma_x = \sigma_y = 4 \ \mu\text{m},$$

so that the typical luminosity has been $\sim 3 \times 10^{27}$ cm^{-2}sec^{-1}.

In the Standard Model, the cross section for production of visible hadronic events (as opposed to lepton or neutrino events), σ_{had}, at the mass of the Z^0 is $\sigma_{\text{had}}(Z^0) \simeq 30$ nb. Thus the measured luminosity can be expressed in terms of the equivalent Z^0 yield (at the peak of the cross section). Figure 6 shows the daily yield of Z^0's to date, while the integrated yield is shown in fig. 7. A yield of 3 Z^0/day has been typical when the SLC has been operational.

III. THE MARK II AT THE SLC

A representation of the MARK II detector is shown in fig. 8. while a more schematic view is given in fig. 9. Aside from detector elements described[2] for the upgraded MARK II at PEP, there are two additional new detector elements for the measurements to be presented today.

The Small Angle Monitors (SAMs) are electromagnetic calorimeters with upstream tracking chambers placed symmetrically at ± 1.5 m along the beam line. Figure 10 shows a SAM surrounding the beam pipe, subtending polar angles of 40–140 mrad. The cross section for bhabha events within the SAM acceptance is 42 nb, a rate comparable (1.4 times) to the Z^0 rate at the Z^0 peak. At the present time systematic errors in the luminosity deduced from the SAM yield are dominated by the statistical error.

The luminosity inferred from the SAM bhabhas is compared in fig. 11 to that from the beam-beam deflection (B-B defl.). Each scan point is for data at a different center of mass energy (see Table 1 below). No systematic bias is discernible in this data. (Also shown in this figure are comparisons with a still smaller, 14–25 mrad, bhabha detector, the mini-SAM;

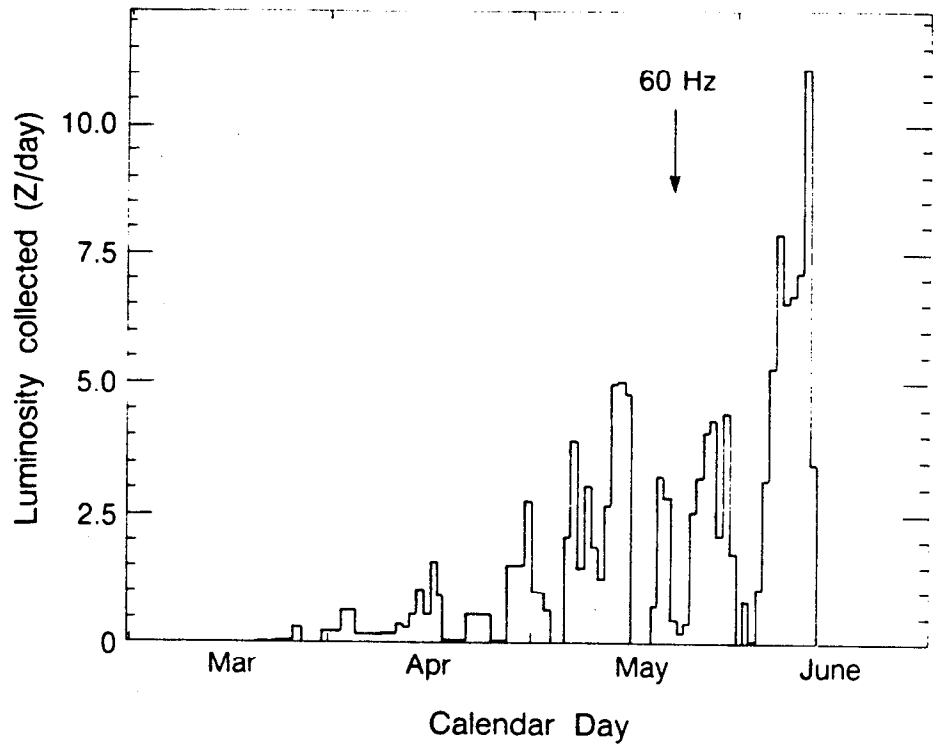

XBL 897-7199

Fig. 6. Daily luminosity, expressed as the number of Z^0 hadronic events which would be produced at the energy set to the mass of the Z^0.

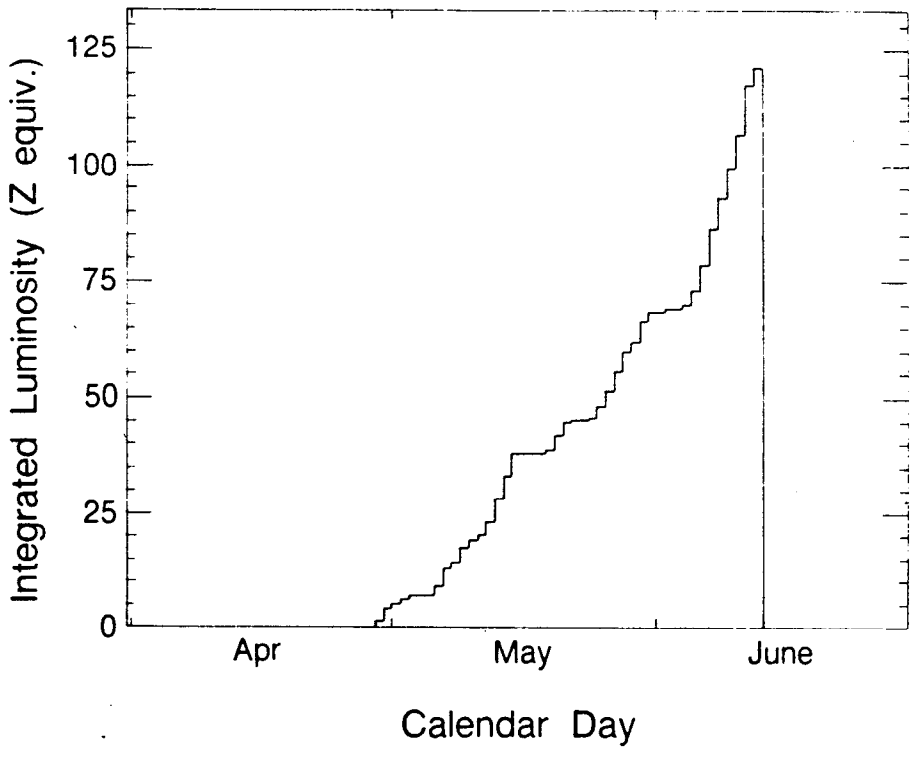

XBL 897-7202

Fig. 7. Integrated luminosity for this running period.

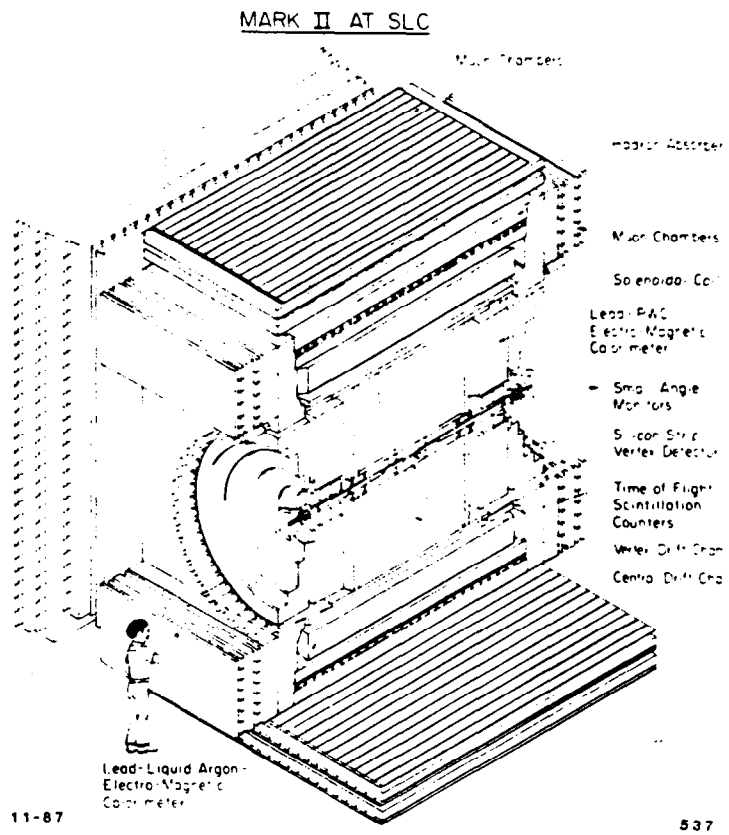

Fig. 8. Pictorial representation of the MARK II at the SLC.

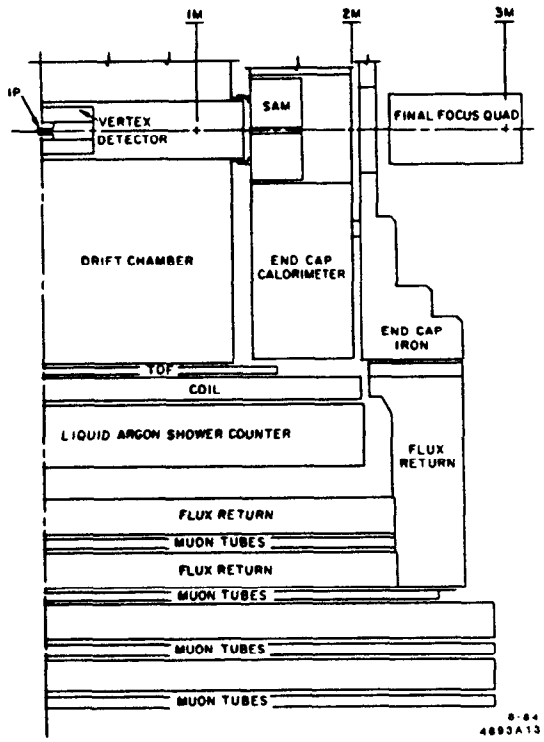

Fig. 9. Schematic representation of the MARK II.

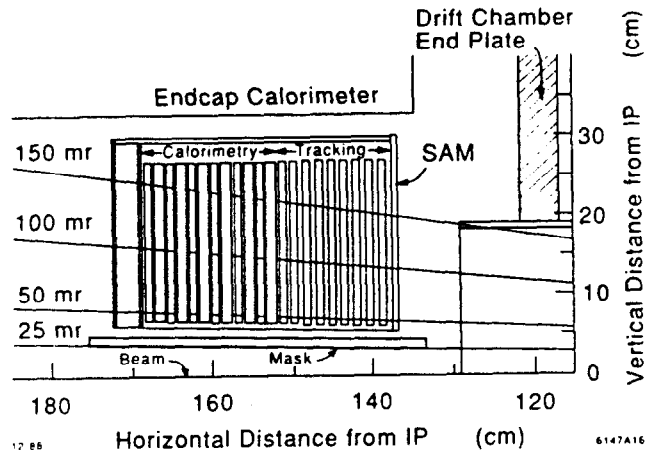

Fig. 10. Schematic drawing of a small angle monitor.

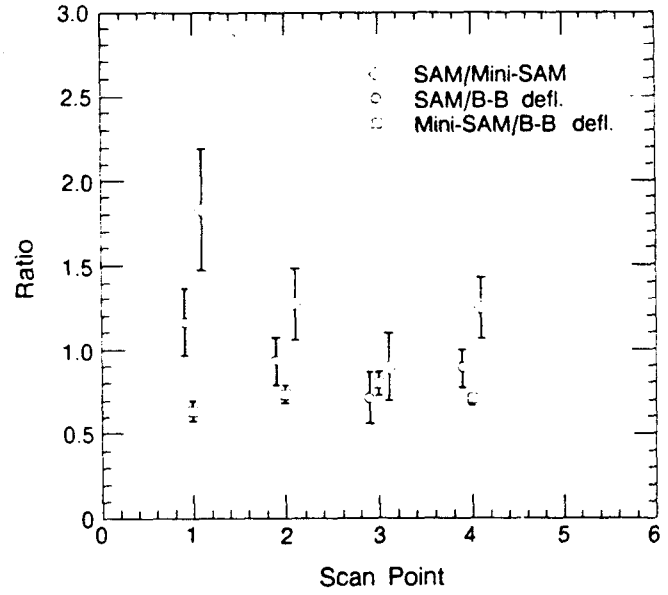

Fig. 11. Luminosity ratios for the various luminosity measuring devices.

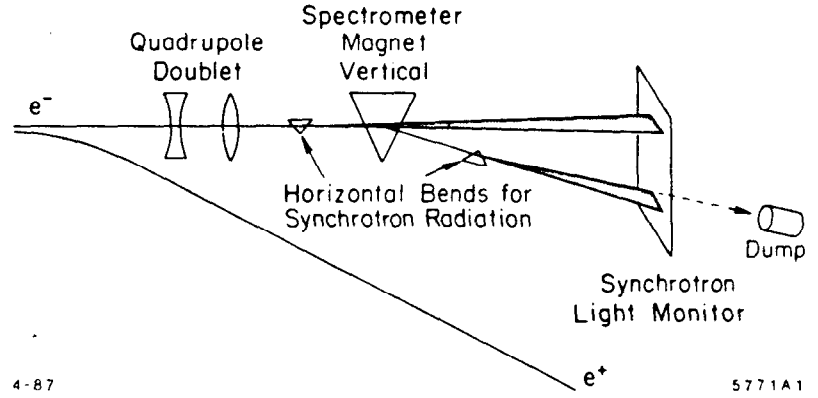

Fig. 12. Extraction line spectrometer used to determine the absolute e^- energy.

these measurements are currently plagued by background problems, and more especially by alignment uncertainties, and will not be used in this report.)

The other new detector is the extraction line spectrometer, shown in fig. 12. The spent e^- is kicked by a pulsed magnet into the extraction line towards the e^- beam dump, passing through a precision spectrometer. Horizontal bends both upstream and downstream of the spectrometer magnet yield synchrotron radiation that impinges on a phosphorescent screen as horizontal stripes. The distance between these stripes may be accurately measured using standard television cameras and digitizers, so that the accurately mapped vertical bending can be converted into an absolute momentum measurement. The systematic error that this device contributes to a mass determination of the Z^0 in a 5-point scan near the Z^0 mass is $\simeq$ 40 MeV. Present statistics can safely ignore systematic errors of this level.

IV. DATA SAMPLE

The trigger used by the MARK II has both a charged and a neutral input, logically OR-ed. The charged trigger requires 2 tracks, separated by at least 11° in azimuth, each with at least 8 hits in the innermost 11 drift chamber layers. For $|\cos\theta| < 0.65$, the single track efficiency is greater than 99%. A Monte Carlo simulation of hadronic events at the Z^0 mass gives a hadronic detection efficiency of 97% (with the losses occurring due to events at small polar angles).

The neutral trigger uses signals in the liquid argon and endcap electromagnetic calorimeters to form software towers, with thresholds of 7 and 5 GeV, respectively. The efficiency of hadronic events is determined by the Monte Carlo to be 92%.

The combined efficiency of the two triggers is 99.4%. Of the first 73 hadrons observed, all satisfied the charged trigger, and only two failed the neutral criterion (97% success rate). Our trigger efficiency is thus well understood.

To select hadronic events, we start with selection criteria for charged tracks and showers. The tracks are required to have a 1 cm distance of closest approach in the transverse (XY) plane, and a 3 cm distance in space, all reckoned from the measured Interaction Point (determined from the vertex fits of our hadronic sample). For showers we use all energy clusters with measured $E > 1$ GeV (after special pattern recognition is used to suppress background $\mu^\pm$ tracks in the LA calorimeter).

With these criteria, we plot in fig. 13a the charged multiplicity ("tracks") for all events on a summary tape of extremely loose cuts. We compare this distribution to fig. 13c which is derived from a Monte Carlo sample of Z^0 decays. We see that a cut of events with fewer than 3 tracks loses a small fraction of the Monte Carlo sample, and eliminates a large background.

The remaining backgrounds in the hadronic sample are mostly due to beam-gas and two-photon events. These backgrounds tend to produce hadrons preferentially in only one

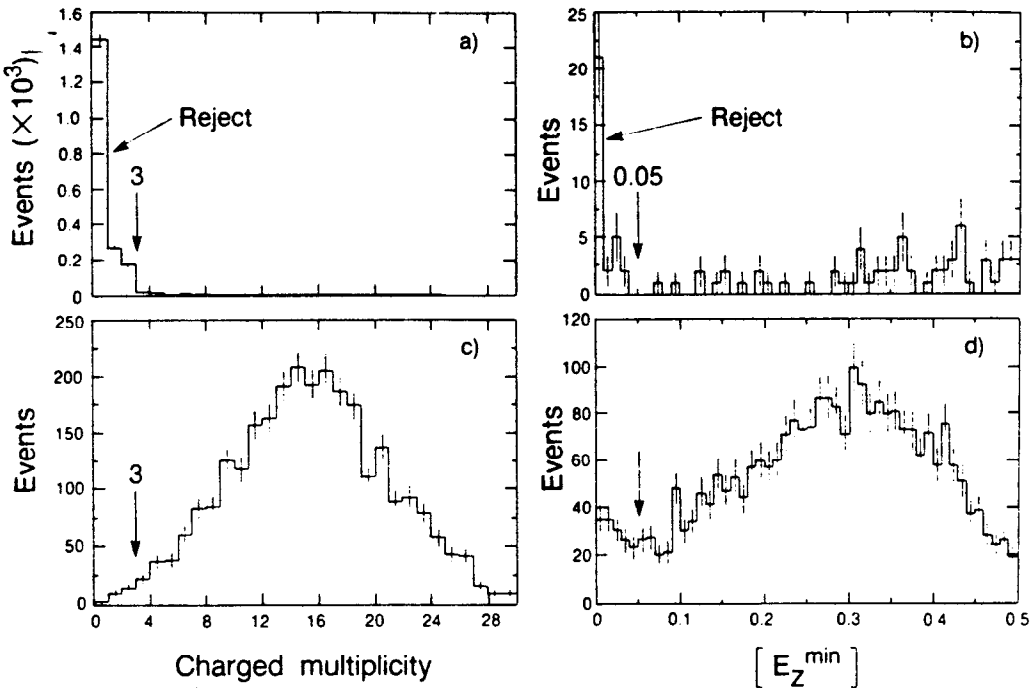

Fig. 13. Charged multiplicity and $E_Z{}^{\min}$ (see text) distributions for data (a,b), and Monte Carlo (c,d), respectively.

hemisphere due to the motion of the center of mass system. To remove these backgrounds, we first form the sums:

$$E_Z^{\pm} = \sum E \text{ (tracks, showers moving in } \pm Z \text{ direction)}$$

(π mass used for tracks).

Then we form

$$E_Z{}^{\min} = \min\{E_Z^+, E_Z^-\}/E_{CM}$$

and require

$$E_Z{}^{\min} > 0.05.$$

Figures 13b and d compare the $E_Z{}^{\min}$ distributions for our data and Monte Carlo, respectively (the multiplicity cut is performed first). The efficiency for these hadronic cuts from the Monte Carlo studies is 94%, with negligible residual background.

V. REPRESENTATIVE EVENTS

The first Z^0 hadronic decay observed by the MARK II is shown in fig. 14. Both the Liquid Argon (LA) and Drift Chamber (DC) system are corrupted by the presence of background hits, but the imprint of the underlying event is unmistakable. Somewhat suspicious in this

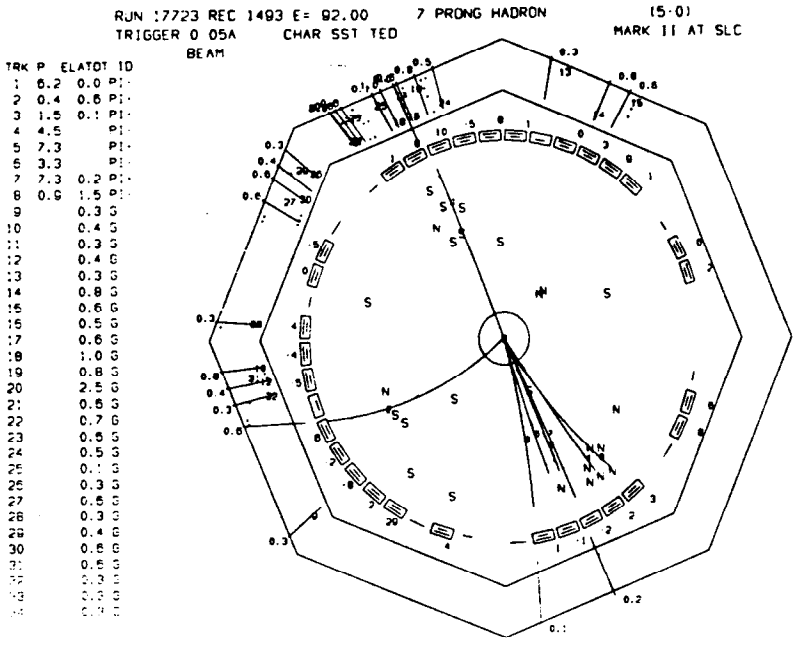

Fig. 14. Transverse view of the central drift chamber and octagonal liquid argon calorimeter for the first hadron observed by the MARK II at the SLC.

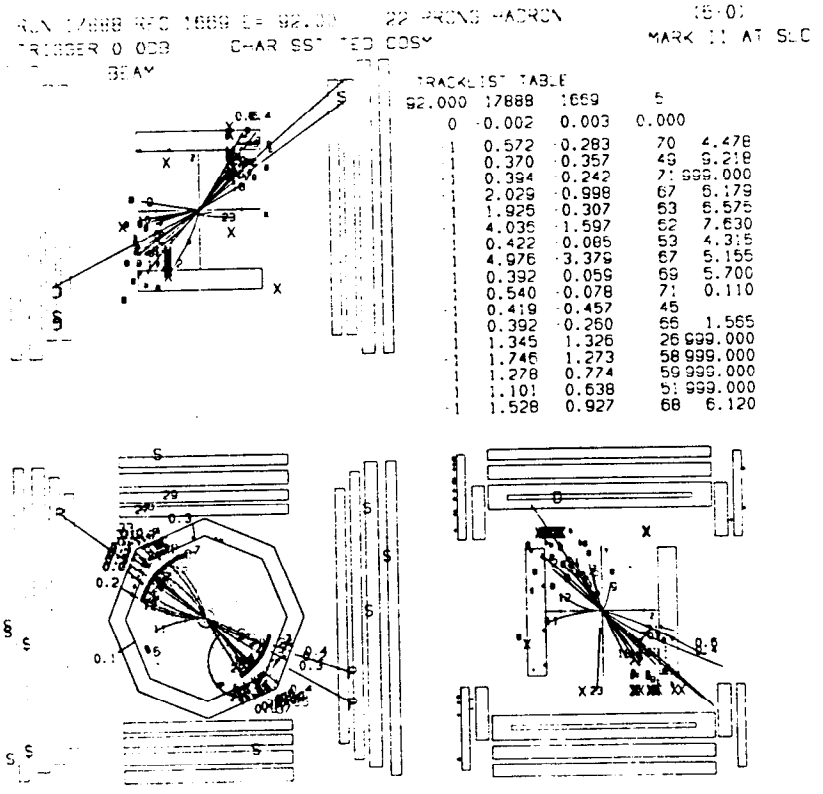

Fig. 15. "Typical" hadronic event in the MARK II detector at the SLC, showing the 3 orthographic projections of the entire detector, including the muon system.

event is the rather small charged multiplicity in the upper hemisphere (the LA activity nearby is background related, showing up in other events recorded close in time to this one).

These suspicions are quickly dispelled by the "typical" event shown in fig. 15 (even though it took $\sim 1/2$ dozen events after the first to find one that looked typical). The leggo version of this event is shown in fig. 16; a clean two-jet structure is apparent.

It is of interest to look at the events which are closest to the ${E_Z}^{\min}$ cut. Figure 17 shows the Z^0 which is closest to failing the cut (${E_Z}^{\min} = 0.07$), while fig. 18 shows the closest discarded event (with ${E_Z}^{\min} = 0.039$). A qualitative difference is difficult to discern. This appears to be due to the events' production angle: as expected, the information we have in the extreme forward and backward regions is poor in quality.

Leptonic events are also seen clearly by the MARK II. Figure 19 shows an e^+e^- in the endcaps (labelled N and S in the figure). Here the charged tracks at small angle and the large energy deposits in the endcaps are well-reconstructed. A $3+3$ $\tau^+\tau^-$ candidate is shown in fig. 20, while a clean $\mu^+\mu^-$ is shown in fig. 21.

Finally, fig. 22 shows the leggo plot from a high multiplicity event: a multi-jet structure is apparent.

VI. ENERGY SCAN, MASS AND WIDTH OF THE Z^0

A summary of the first 5 scan points in an energy survey near the Z^0 mass is given in Table 1 (in fact the 5^{th} point was the result of a last-moment Bitnet message during the conference). The e^+e^- contribution from amplitudes other than the Z^0 pole term is not negligible as it is for the other reactions. We therefore ignore for this analysis the e^+e^- wide-angle events and include in the Z^0 sample the hadronic events, the $\mu^+\mu^-$ and the $\tau^+\tau^-$.

The cross section for these processes, labelled σ_{fiducial}, as a function of energy, is shown in fig. 23. Several curves with line-shapes determined by a Breit-Wigner resonance shape modified by radiative effects are shown for reference. The curve labelled $N_\nu = 3$ assumes that a 91 GeV Z^0 has a width appropriate to the expected couplings to the presently known 3 generations.

For comparison, a curve $N_\nu = 4$ assumes that a 4th generation massless $\nu\bar{\nu}$ is produced (and that the other members of the generation are too heavy to be kinematically accessible). The curve b' retains the $N_\nu = 3$ assumption, but allows a 30 GeV b' to decay detectably.

Inspection shows that our ability to distinguish between alternatives is rather poor at present. What can we say with some degree of certainty?

Firstly, that the SLC has turned on for physics, albeit at a rate close to our worst expectations. Second, that with the first ~ 100 events in hand, there are no surprises thus far. Lastly, the scan in energy for the mass and width of the Z^0 is in progress. So far, 91 GeV is looking good.

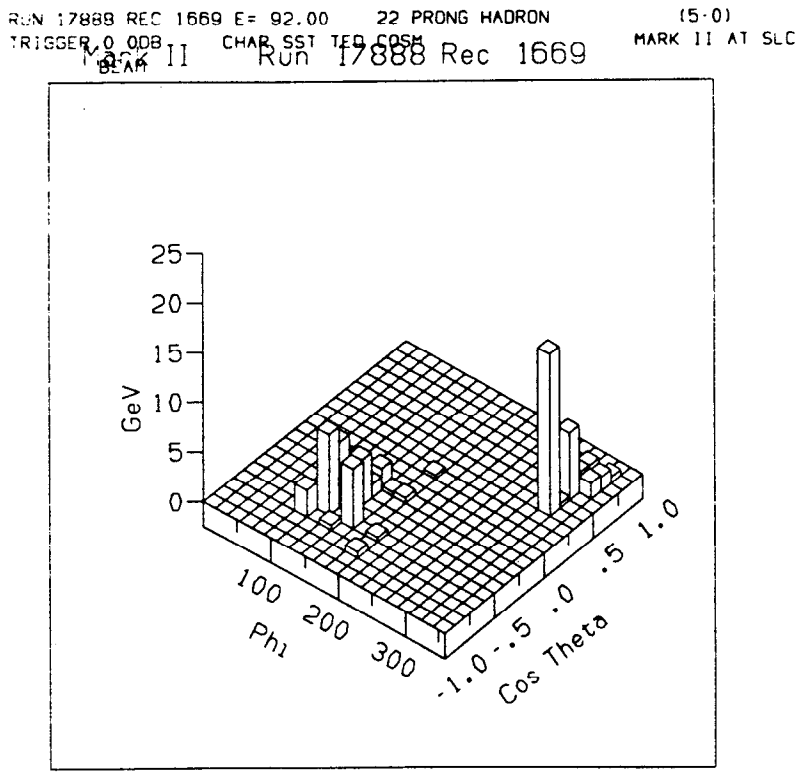

Fig. 16. A leggo plot (γ vs. $\cos\theta$ 2-dimensional histogram) for the event shown in fig. 15.

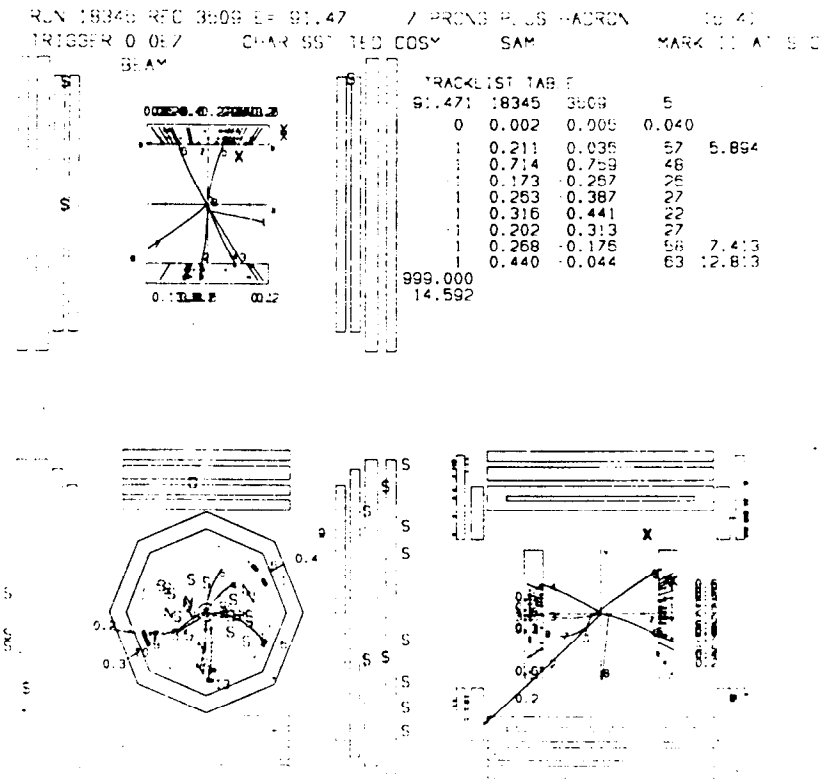

Fig. 17. Accepted Z^0 hadron closest to failing the $E_Z{}^{\min}$ cut.

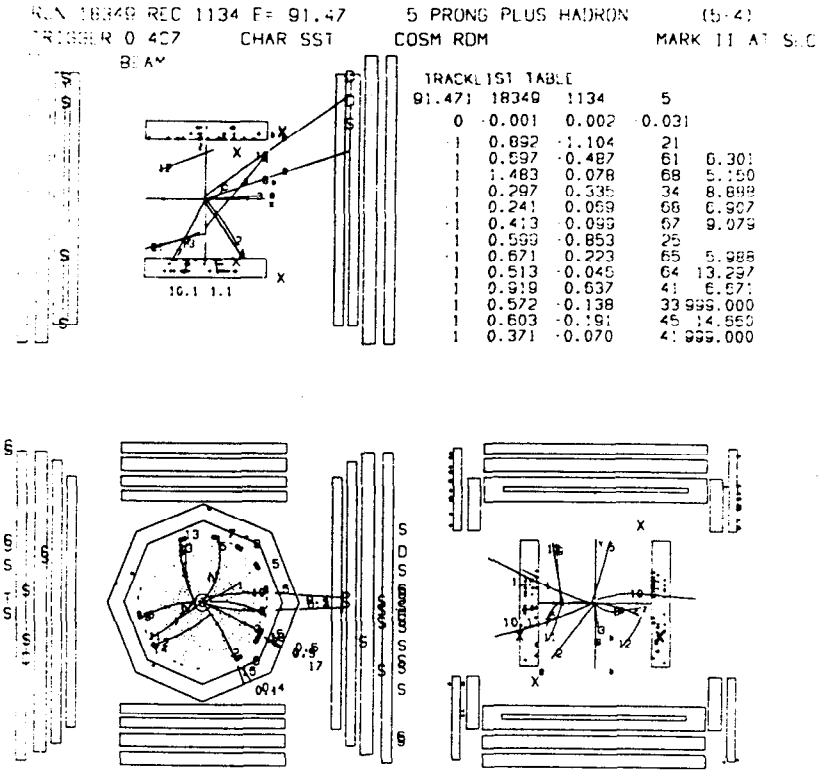

Fig. 18. Discarded event closest to passing the $E_Z{}^{\min}$ cut.

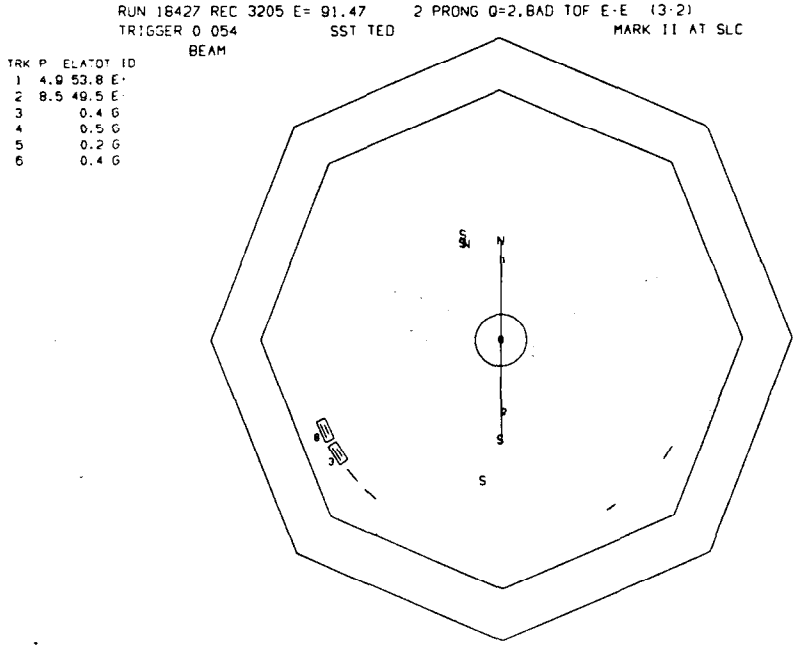

Fig. 19. Endcap e^+e^- event.

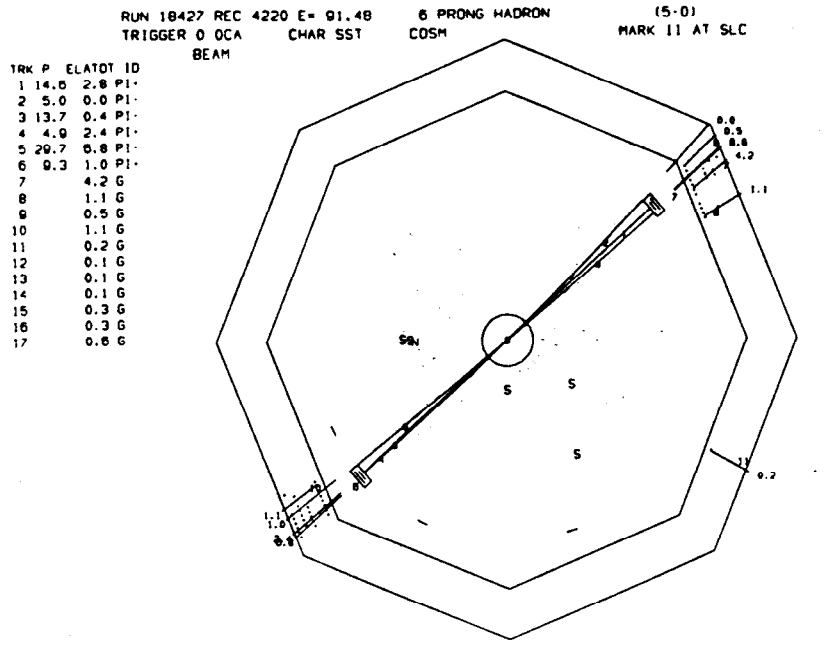

Fig. 20. A $3+3$ $\tau^+\tau^-$ candidate.

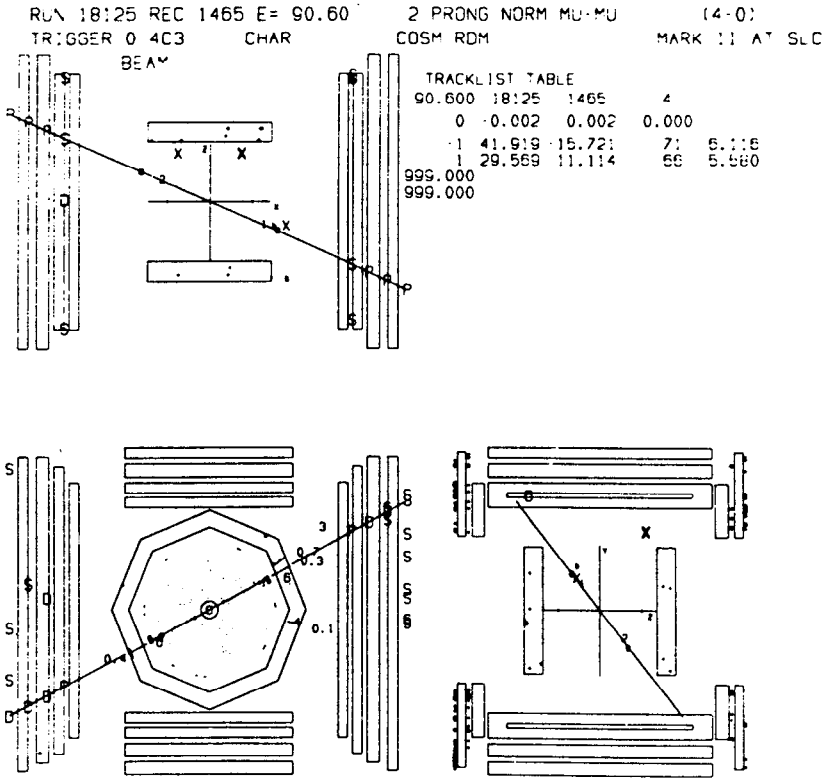

Fig. 21. A $\mu^+\mu^-$ candidate.

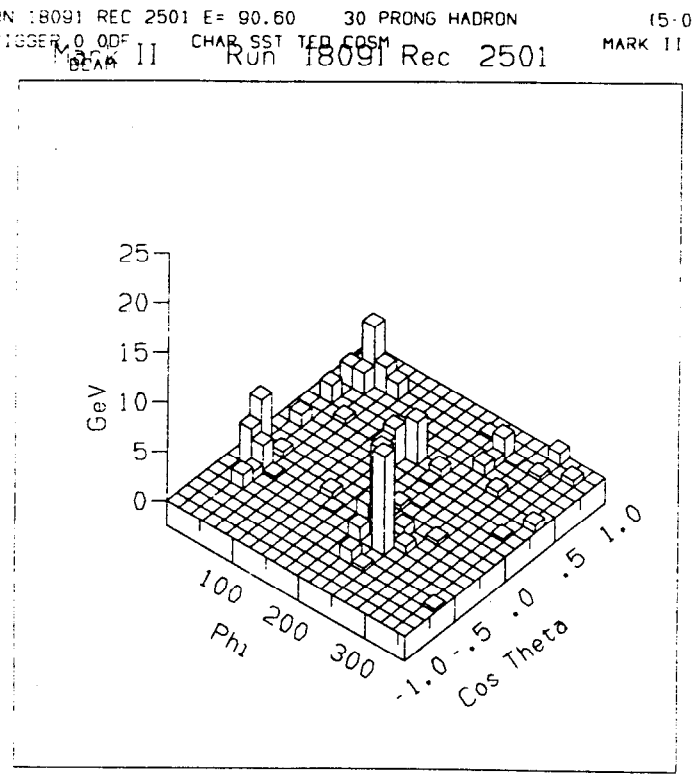

Fig. 22. Leggo plot of a high multiplicity event.

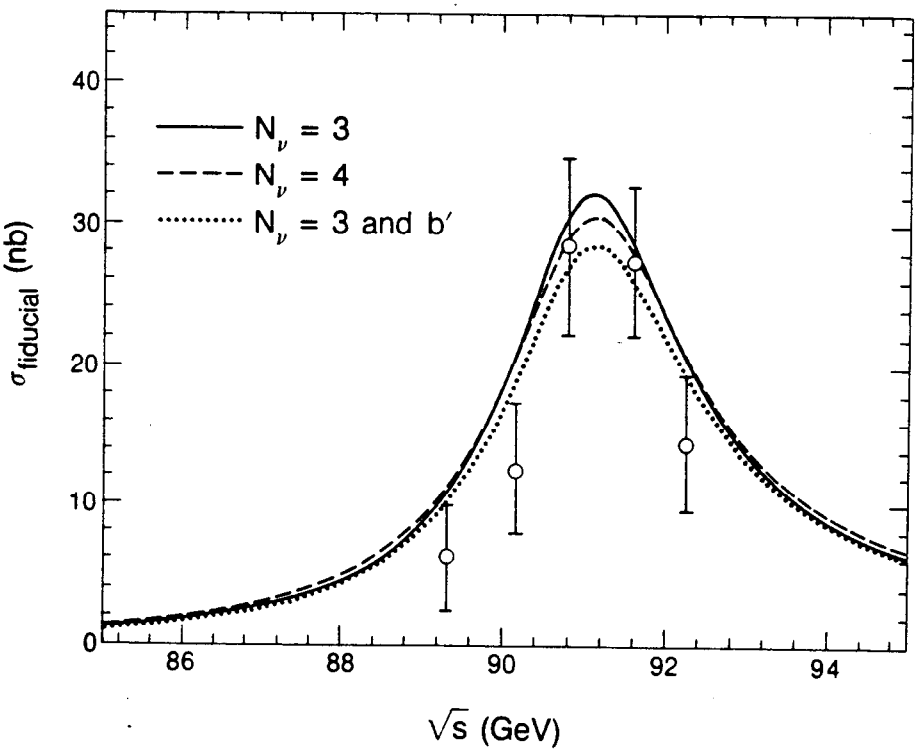

Fig. 23. Cross section for hadronic, $\mu^+\mu^-$ and $\tau^+\tau^-$ events as a function of center of mass energy.

TABLE 1
Event Summary of the First 5 Scan Points

			Z			
Point	$\sqrt{s}$ (GeV)	e^+e^- (SAM)	Hadrons	$\mu^+\mu^-$	$\tau^+\tau^-$	e^+e^-
1	92.2	34	11	0	0	0
2	90.7	45	27	2	1	1
3	89.2	24	3	0	0	0
4	91.4	61	32	1	7	1
5	90.1	38	8	1	1	0
	Total	202	81	4	9	2

REFERENCES

1. Members of the MARK II Collaboration. Lawrence Berkeley Laboratory: G.S. Abrams, S. Bethke, G. Gidal, G. Goldhaber, R. Harr, C. Hearty, J. Kadyk, F. Kral, M. Levi, G. Lynch, F. Rouse, M. Schaad, A. Schumm, and G. Trilling. California Institute of Technology: B. Barish, C. Hawkes, M. Kuhlen, J. McKenna, B. Milliken, C. Peck, F. Porter, E. Soderstrom, R. Stroynowski, A. Weinstein, A. Weir, E. Wicklund, and D. Wu. University of Colorado: W.T. Ford, D. Hinshaw, P. Rankin, J. Smith, S. Wagner, and P. Weber. University of Hawaii: A. Breakstone, R. Cence, F. Harris, and S. Parker. Indiana University: D. Averill, D. Blockus, B. Brabson, W. Murray, H. Ogren, D. Rust, A. Snyder, and M. Yurko. Johns Hopkins University: B. Barnett, D. Drewer, P. Dauncey, B. Harral, J. Hylen, J. Matthews, and D. Stoker. University of Michigan, Ann Arbor: G. Bonvicini, J. Chapman, M. Chmeissani, R. Frey, E. Gero, S. Hong, W. Koska, M. Petradza, and R. Thun. University of California, Santa Cruz: C. Adolphsen, P. Burchat, D. Dorfan, C. Gatto, G. Gratta, J. Gomez-Cadenas, C. Heusch, J. Kent, M. King, L. Labarga, A. Litke, H. Sadrozinski, A. Seiden, C. Von Zanthier, S. Watson, and C. Zaccardelli. Stanford Linear Accelerator Center: J. Ballam, J. Bartelt, T. Barklow, A. Boyarski, F. Bulos, D. Burke, D. Cords, D. Coupal, H. DeStaebler, J. Dorfan, R. Elia, G. Feldman, R. Field C. Fordham, D. Fujino, K.K. Gan, T. Glanzman, G. Grindhammer, G. Hanson, K. Hayes, T. Himel, D. Hutchinson, W. Innes, R. Jacobsen, J. Jaros, C.-K. Jung, D. Koetke, S. Komamiya, A.L. Kowalski, W. Kozanecki, A. Lankford, R. Larsen, F. LeDiberder, V. Luth, T. Mattison, K. Moffeit, C. Munger, J. Nash, K. O'Shaughnessy, M. Perl, R. Pitthan, K. Riles, M. Swartz, R. Taylor, R. Van Kooten, and M. Woods. This work was supported by the Director, Office of Energy Research, Office of High Energy and Nuclear Physics, Division of High Energy Physics of the U.S. Department of Energy under Contract Number DE-AC03-76SF00098.
2. G. Abrams et al., "The MARK II Detector for the SLC", submitted to NIM, Feb. 1989.